Available online at www.sciencedirect.com
SCIENCE DIRECT
International Journal of Heat and Mass Transfer 49 (2006) 4469–4481
International Journal of HEAT and MASS TRANSFER
www.elsevier.com/locate/ijhmt

Temperature dependent viscosity effects on laminar forced convection in the entrance region of straight ducts

C. Nonino *, S. Del Giudice, S. Savino

Dipartimento di Energetica e Macchine, Università degli Studi di Udine, Via delle Scienze 208, 33100 Udine, Italy

Received 5 December 2005
Available online 25 July 2006

Abstract

A parametric investigation is carried out on the effects of temperature dependent viscosity in simultaneously developing laminar flow of a liquid in straight ducts of arbitrary but constant cross-sections. Viscosity is assumed to vary with temperature according to an exponential relation, while the other fluid properties are held constant. Different cross-sectional geometries are considered, corresponding both to three-dimensional (rectangular, trapezoidal and hexagonal) and to axisymmetric (circular and concentric annular) duct geometries. Uniform wall temperature boundary conditions are imposed on the heated/cooled walls of the ducts. A finite element procedure is employed for the solution of the parabolized momentum and energy equations. Computed axial distributions of the local Nusselt number and of the apparent Fanning friction factor for ducts of the considered cross-sections are presented with reference to both fluid heating and fluid cooling. Numerical results confirm that, in the laminar forced convection in the entrance region of straight ducts, the effects of temperature dependent viscosity cannot be neglected in a wide range of operative conditions.

Keywords: Laminar forced convection; Straight ducts; Entrance region; Temperature dependent viscosity

1. Introduction

In many duct flows of practical interest, velocity and temperature fields develop simultaneously, resulting in overlapping hydrodynamic and thermal entrance regions. This occurs when fluid heating or cooling begins at the duct inlet, where the velocity boundary layer also starts developing. In such a situation, entrance effects on fluid flow and forced convection heat transfer cannot be neglected if, as it happens quite often in laminar flows, the total length of the duct is comparable with that of the entrance region. Moreover, temperature dependence of fluid properties can also play an important role in the development of the velocity and temperature fields. If the fluid is a liquid, viscosity is the property which exhibits the most relevant variations with respect to temperature. Therefore, the main effects of temperature dependent fluid properties can be retained even if only viscosity is allowed to vary with temperature, while the other properties are assumed constant. Even if these effects have already been considered in the past, to the authors' knowledge no systematic studies are reported in the literature taking into account the combination of entrance and temperature dependent viscosity effects.

In the past decades, many authors have investigated, both analytically and numerically, simultaneously developing flows in straight ducts of constant cross-section. Comprehensive reviews of these theoretical studies, referring to ducts of different cross-sectional geometries, can be found in [1,2]. However, since a basic assumption made in almost all such studies is that fluid properties are constant, the corresponding solutions are adequate only for problems involving small temperature differences. In fact, experimental results for problems involving large temperature differences substantially deviate from constant property solutions [1,3]. However, it must be

* Corresponding author. Tel.: +39 0432 558019; fax: +39 0432 558027.
E-mail address: carlo.nonino@uniud.it (C. Nonino).

0017-9310/$ - see front matter © 2006 Elsevier Ltd. All rights reserved.
doi:10.1016/j.ijheatmasstransfer.2006.05.021

Nomenclature

A	area of the cross-section (m^2)
a	height of the cross-section (m)
B	parameter in Eq. (13) ($=-\ln(\mu_e/\mu_w)$)
b	base of the cross-section (m)
c	specific heat (J/kg K)
D_h	hydraulic diameter (m)
f	Fanning friction factor (–)
h	local convection coefficient (W/m^2 K)
k	thermal conductivity (W/m K)
Nu	Nusselt number ($=hD_h/k$)
P	perimeter of the cross-section (m)
P_t	heated/cooled perimeter (m)
Pe	Péclet number ($=Re\,Pr$)
Pr	Prandtl number ($=\mu c/k$)
p	deviation from the hydrostatic pressure (Pa)
q'	heat transfer rate per unit length (W/m)
q''	heat flux (W/m^2)
R	dimensionless radial coordinate ($=r/r_o$)
Re	Reynolds number ($=\rho u_e D_h/\mu$)
r	radial coordinate (m)
T	dimensionless temperature ($=(t-t_w)/(t_e-t_w)$)
T'	dimensionless temperature ($=(t-t_w)/(t_b-t_w)$)
t	temperature (°C)
U	dimensionless axial velocity ($=u/u_e$)
u, v, w	velocity components (m/s)
X^+	dimensionless axial coordinate ($=x/D_hRe_m$)
X^*	dimensionless axial coordinate ($=x/D_hPe$)
x	axial coordinate (m)
y, z	transverse Cartesian coordinates (m)
Z	dimensionless transverse coordinate ($=z/D_h$)

Greek symbols

β	parameter in Eq. (12) (1/K)
γ	aspect ratio of the cross-section ($=a/b$)
μ	dynamic viscosity (kg/m s)
ρ	density (kg/m^3)

Subscripts and superscripts

0	centerline
a	apparent
b	bulk
c	constant property
e	entrance
i	inner
m	reference, evaluated at t_m
o	outer
w	wall
–	average value
∞	asymptotic value

mentioned that, for engineering applications, the effects of property variations are usually taken into account by adjusting constant property solutions by means of correction factors with only limited empirical and theoretical justification, thus leading to some ambiguity and awkwardness [1].

As anticipated above, for most liquids, density, specific heat and thermal conductivity are nearly independent of temperature, while viscosity markedly decreases with increasing temperature, in much the same manner as the Prandtl number does [3]. Thus, the constant property assumption, with the exception of viscosity, which is still allowed to vary with temperature, is adequate for most liquid flows, no matter how large the temperature differences are. Because of the relative complexity of temperature dependent property problems, only a limited number of such solutions for laminar forced convection in simultaneously developing flow in ducts have appeared in the literature [1]. However, most of these studies are based on the assumption of a viscosity dependence on temperature given by a specific relation of empirical nature [3–7], leading to results which cannot be considered general and applicable to other liquids or for different temperature ranges. Similar considerations can be made with respect to studies concerning thermally or simultaneously developing flows in microchannels [8–11].

In this paper, we present the results of a parametric study on the simultaneously developing laminar flow of a liquid in straight ducts of arbitrary, but constant, cross-sections. The effects of temperature dependent viscosity on pressure drop and heat transfer are investigated, while the other liquid properties are considered constant. An extended version of the finite element procedure described in [12] is employed for the step-by-step solution of the parabolized momentum and energy equations [13,14] in a two-dimensional domain corresponding to the cross-section of the duct. In most situations of practical interest, because of the high value of the ratio between the total length and the hydraulic diameter, such an approach is very advantageous with respect to the one based on the steady-state solution of the elliptic form of the governing equations in a three-dimensional domain corresponding to the whole duct. New results concern different cross-sectional geometries, chosen among those usually adopted for ducts (circular, rectangular and concentric annular [1]) and for microchannels (trapezoidal and hexagonal [15,16]). In all the cases studied here, reference is made to uniform wall temperature boundary conditions, while viscosity is assumed to have an exponential variation with temperature in the range considered [3,6,7,17–19]. In order to allow a parametric investigation, a suitable dimensionless form of the assumed viscosity-temperature relation is used.

2. Mathematical model and numerical procedure

When the effects of axial diffusion can be neglected and there is no recirculation in the longitudinal direction, steady-state flow and heat transfer in straight ducts of constant cross-sections are governed by the continuity equation and by the parabolized Navier–Stokes and energy equations [13,14]. Since the inverse of the Reynolds number is representative of the relative importance of diffusive and advective components of the axial momentum flow rate, while the inverse of the Péclet number is representative of the relative importance of conductive and advective components of the axial heat flow rate, the parabolic approximation of the Navier–Stokes and energy equations can be considered adequate, except in the immediate neighborhood of the inlet, for values of the Reynolds and Péclet numbers larger than 50 [1,20].

With reference to incompressible fluids with temperature dependent thermophysical properties, in the hypotheses of negligible body forces and negligible viscous dissipation, the above mentioned equations can be written in the following forms, valid for three-dimensional and axisymmetric geometries, respectively. For three-dimensional duct geometries, the governing equations are

$$\frac{\partial}{\partial x}(\rho u)+\frac{\partial}{\partial y}(\rho v)+\frac{\partial}{\partial z}(\rho w)=0 \tag{1}$$

$$\rho u\frac{\partial u}{\partial x}=\frac{\partial}{\partial y}\left(\mu\frac{\partial u}{\partial y}\right)+\frac{\partial}{\partial z}\left(\mu\frac{\partial u}{\partial z}\right)-\rho v\frac{\partial u}{\partial y}-\rho w\frac{\partial u}{\partial z}-\frac{\mathrm{d}\bar{p}}{\mathrm{d}x} \tag{2}$$

$$\rho u\frac{\partial v}{\partial x}=\frac{\partial}{\partial y}\left[2\mu\frac{\partial v}{\partial y}-\frac{2}{3}\left(\mu\frac{\partial v}{\partial y}+\mu\frac{\partial w}{\partial z}\right)\right]+\frac{\partial}{\partial z}\left(\mu\frac{\partial w}{\partial y}+\mu\frac{\partial v}{\partial z}\right)-\rho v\frac{\partial v}{\partial y}-\rho w\frac{\partial v}{\partial z}-\frac{\partial p}{\partial y} \tag{3}$$

$$\rho u\frac{\partial w}{\partial x}=\frac{\partial}{\partial z}\left[2\mu\frac{\partial w}{\partial z}-\frac{2}{3}\left(\mu\frac{\partial v}{\partial y}+\mu\frac{\partial w}{\partial z}\right)\right]+\frac{\partial}{\partial y}\left(\mu\frac{\partial w}{\partial y}+\mu\frac{\partial v}{\partial z}\right)-\rho v\frac{\partial w}{\partial y}-\rho w\frac{\partial w}{\partial z}-\frac{\partial p}{\partial z} \tag{4}$$

$$\rho cu\frac{\partial t}{\partial x}=\frac{\partial}{\partial y}\left(k\frac{\partial t}{\partial y}\right)+\frac{\partial}{\partial z}\left(k\frac{\partial t}{\partial z}\right)-\rho cv\frac{\partial t}{\partial y}-\rho cw\frac{\partial t}{\partial z} \tag{5}$$

while, for axisymmetric duct geometries, they become

$$\frac{\partial}{\partial x}(\rho u)+\frac{1}{r}\frac{\partial}{\partial r}(\rho rv)=0 \tag{6}$$

$$\rho u\frac{\partial u}{\partial x}=\frac{1}{r}\frac{\partial}{\partial r}\left(\mu r\frac{\partial u}{\partial r}\right)-\rho v\frac{\partial u}{\partial r}-\frac{\mathrm{d}\bar{p}}{\mathrm{d}x} \tag{7}$$

$$\rho u\frac{\partial v}{\partial x}=\frac{2}{r}\left[\frac{\partial}{\partial r}\left(\mu r\frac{\partial v}{\partial r}\right)-\mu\frac{v}{r}\right]-\frac{2}{3r}\left\{\frac{\partial}{\partial r}\left[\mu\frac{\partial}{\partial r}(rv)\right]+\frac{\mu}{r}\frac{\partial}{\partial r}(rv)\right\}-\rho v\frac{\partial v}{\partial r}-\frac{\partial p}{\partial r} \tag{8}$$

$$\rho cu\frac{\partial t}{\partial x}=\frac{1}{r}\frac{\partial}{\partial r}\left(kr\frac{\partial t}{\partial r}\right)-\rho cv\frac{\partial t}{\partial r} \tag{9}$$

According to the assumption of parabolic flow, all the derivatives in the axial direction are neglected in the diffusive terms of the above equations [14]. In the set of equations valid for three-dimensional geometries, x, y and z are the axial and the transverse coordinates, respectively, while u, v and w represent the axial and the transverse components of velocity. In the axisymmetric equations, symbols r and v denote the radial coordinate and the radial component of velocity. Finally, t is the temperature, p is the deviation from the hydrostatic pressure, $\bar{p}$ is its average value over the cross-section, while ρ, μ, c and k represent density, dynamic viscosity, specific heat and thermal conductivity of the fluid, respectively.

The solution domain can be bounded by rigid walls or symmetry axes. The usual no-slip conditions are applied on rigid boundaries, that is, $u=v=w=0$ for three-dimensional geometries and $u=v=0$ in the axisymmetric cases, while either the temperature is prescribed ($t=t_w$) or the wall is assumed adiabatic ($\partial t/\partial n=0$). Symmetry conditions, instead, are $\partial u/\partial y=\partial w/\partial y=0$, $v=0$ and $\partial t/\partial y=0$ on boundaries perpendicular to the y axis, $\partial u/\partial z=\partial v/\partial z=0$, $w=0$ and $\partial t/\partial z=0$ on boundaries perpendicular to the z axis for three-dimensional geometries, and $\partial u/\partial r=0$, $v=0$ and $\partial t/\partial r=0$ at the symmetry axis in axisymmetric problems.

The model equations are solved using a finite element procedure which represents an extended version of the one previously developed for the analysis of the forced convection of constant property fluids in the entrance region of straight ducts [12]. The added new features mainly consist in the possibility of analyzing flows of incompressible fluids with temperature dependent properties. The adopted procedure is based on a segregated approach which implies the sequential solution of the momentum and energy equations on a two-dimensional domain in the case of three-dimensional geometries and on a one-dimensional domain in axisymmetric problems. A marching method is then used to move forward in the axial direction of the duct. The pressure–velocity coupling is dealt with using an improved projection algorithm already employed by one of the authors (C.N.) for the solution of the Navier–Stokes equations in their elliptic form [21].

Most of the features of the adopted solution algorithm and of the finite element discretization procedure can be found in [12], where reference is made to a constant property fluid and to the dimensionless forms of the governing equations. Since this description can be easily adapted to the case of a fluid with temperature dependent properties considered here, only the details concerning the estimation of the average pressure gradient $\mathrm{d}\bar{p}/\mathrm{d}x$, which is necessary to solve the momentum equation in the axial direction, are reported in this paper. With reference to the flow in straight ducts, integration of the axial momentum equation over the cross-section A gives [1,12]

$$-\frac{\mathrm{d}\bar{p}}{\mathrm{d}x}=\frac{\mathrm{d}}{\mathrm{d}x}\left(\frac{1}{A}\int_A\rho u^2\,\mathrm{d}A\right)-\frac{1}{A}\int_P\mu\frac{\partial u}{\partial n}\mathrm{d}P=\frac{\mathrm{d}K}{\mathrm{d}x}+L \tag{10}$$

In the previous equation P is the perimeter of the cross-section and n denotes the direction of the outer normal to the boundary, while K and L represent the axial momentum

rate and the wall viscous force per unit length, respectively, referred to the unit area of the cross-section. Their definitions can be directly inferred from the above equation. In the marching procedure from the nth to the $(n+1)$th axial locations, the following approximation for the average pressure gradient is used:

$$-\left(\frac{\mathrm{d}\bar{p}}{\mathrm{d}x}\right)^{*} = \left(\frac{\mathrm{d}K}{\mathrm{d}x}\right)^{*} + L^{n} = \frac{1}{2}\left(\frac{K^{n}-K^{n-1}}{x^{n}-x^{n-1}} + \frac{K^{n}-K^{n-2}}{x^{n}-x^{n-2}}\right) + L^{n} \tag{11}$$

where the asterisk (*) indicates an estimated value. The backward formula employed in Eq. (11) for the evaluation of $(\mathrm{d}K/\mathrm{d}x)^{*}$ has been adopted to increase stability since we observed that more accurate second order approximations very often led to the divergence of the simulations. However, it must be pointed out that this choice does not affect the overall accuracy of the numerical results if, as will be detailed later, very small axial steps are adopted where the variations of the axial pressure gradient are significant, that is, in the region very close to the duct entrance.

3. Numerical results

As stated above, laminar forced convection in the entrance region of straight ducts of constant cross-sections with uniform wall temperature t_w is studied. The hypothesis made here is that liquid heating/cooling begins at the duct inlet, where the velocity boundary layer also starts developing. Therefore, at the entrance of the duct, uniform values of the axial velocity u_e and of the temperature t_e are specified as the appropriate inlet conditions.

The dynamic viscosity is assumed to vary with temperature and μ_e and μ_w are its values at t_e and t_w, respectively. The ratio of μ_e over μ_w gives an indication of the relevance of the temperature dependence of viscosity in the range between t_e and t_w. Exponential or Arrhenius type relations are usually employed to represent the temperature dependence of viscosity. The one adopted in this paper is the widely used exponential formula [3,6,7,17–19]

$$\mu = \mu_w \exp[-\beta(t - t_w)] \tag{12}$$

with $\beta = -(\mathrm{d}\mu/\mathrm{d}t)/\mu = \text{const}$. By means of simple manipulations, Eq. (12) can be cast in the following dimensionless forms:

$$\frac{\mu}{\mu_w} = \exp(-BT) = \left(\frac{\mu_e}{\mu_w}\right)^{T} \tag{13}$$

where $T = (t - t_w)/(t_e - t_w)$ is the dimensionless temperature and $B = -\ln(\mu_e/\mu_w)$ is a dimensionless viscosity parameter.

It is worth noting that, since all the other thermophysical properties are assumed constant, we have $\mu_e/\mu_w = Pr_e/Pr_w = Re_w/Re_e$. Moreover, while the local Reynolds number $Re = \rho u_e D_h/\mu$ and the local Prandtl number $Pr = \mu c/k$ depend on temperature, the local Péclet number $Pe = Re\,Pr = Re_e Pr_e = Re_w Pr_w$ always has the same value. Since the viscosity of liquids decreases with increasing temperature, $Pr_e/Pr_w > 1$ corresponds to fluid heating ($t_e < t_w$) and $Pr_e/Pr_w < 1$ to fluid cooling ($t_e > t_w$), while $Pr_e/Pr_w = 1$ refers to isothermal flows ($t_e = t_w$) or to constant viscosity fluids.

In all the computations, the same values $Re_m = \rho u_e D_h/\mu_m = 500$ and $Pr_m = \mu_m c/k = 5$ of the Reynolds and Prandtl numbers at the reference temperature of the fluid $t_m = (t_e + t_w)/2$ have been assumed. The corresponding value of the Péclet number is $Pe = 2500$. Therefore, for the values of the ratio $Pr_e/Pr_w = 1/4$, 1/2, 1, 2 and 4 considered here, minimum and maximum values of the local Reynolds number in the temperature range between t_e and t_w are 250 and 1000, respectively, while the Prandtl number can vary between 2.5 and 10. Fig. 1 illustrates the temperature dependence of the local Prandtl number for the different values of the ratio Pr_e/Pr_w.

In the following, numerical results concerning axial distributions of the local Nusselt number $Nu = hD_h/k$ and of the apparent Fanning friction factor f_a are presented. The local convection coefficient h, averaged over the heated/cooled perimeter of the cross-section, can be computed as

$$h = \frac{q'_w}{P_t(t_b - t_w)} \tag{14}$$

for three-dimensional geometries, and as

$$h = \frac{q''_w}{t_b - t_w} \tag{15}$$

for axisymmetric geometries. In the above equations, q'_w and q''_w are the wall heat transfer rate per unit length and the wall heat flux, respectively, P_t is the heated/cooled perimeter of the cross-section and t_b is the bulk temperature. The apparent Fanning friction factor is defined as [1]

$$f_a = \frac{(\bar{p}_e - \bar{p})D_h}{2\rho u_e^2 x} \tag{16}$$

It must be pointed out that, even if the numerical results reported in the following have been obtained for $Re_m = 500$ and $Pr_m = 5$, they are much more general that what they appear to be. In fact, for a given reference Prandtl number

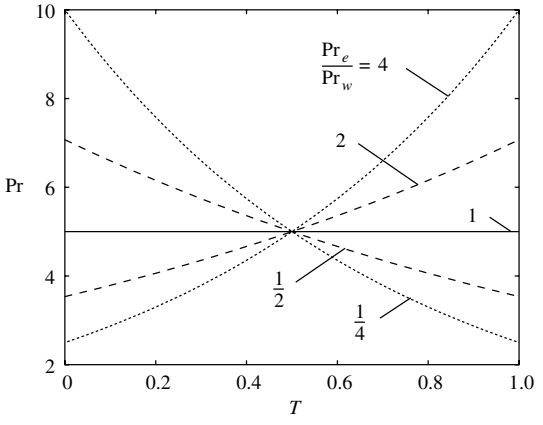

Fig. 1. Graphical representation of the temperature dependence of the local Prandtl number for different values of the ratio Pr_e/Pr_w.

Pr_m, the axial distributions of Nu and f_aRe_m are independent of the reference Reynolds number Re_m provided that the appropriate dimensionless axial coordinates $X^* = x/D_hPe$ or $X^+ = x/D_hRe_m$ are employed. Moreover, the influence of the reference Prandtl number Pr_m on Nu and f_aRe_m distributions is significant only in the first part of the microchannel, i.e., near the entrance. The validity of the above statements, which is well established for constant property flows, has been verified, by means of sample numerical tests, also under the variable viscosity assumption in the ranges $1/4 \leqslant \mu_e/\mu_w \leqslant 4$, $250 \leqslant Re_m \leqslant 1000$ and $2 \leqslant Pr_m \leqslant 20$.

Nine different cross-sectional geometries are considered in this study, corresponding to both three-dimensional and axisymmetric duct geometries. The former group (five geometries) includes rectangular ducts with aspect ratios $\gamma = a/b$ equal to 0 (parallel plates), to 0.5 and to 1 (square duct) and two geometries chosen among those usually adopted for silicon microchannels, namely trapezoidal with $\gamma = a/b = 0.414$ and hexagonal (or double-trapezoidal) with $\gamma = a/b = 0.828$. Symbols a and b denote the height and the width of the cross-section, respectively. The cross-section of the trapezoidal duct is an isosceles trapezium with the larger base b and height a and a 54.74° angle between sides and the larger base, while that of the hexagonal duct corresponds to two of such trapezia joined along the larger base [15,16]. Details of trapezoidal and hexagonal cross-sections are reported in Fig. 2. Axisymmetric geometries include circular ducts and three concentric annular ducts with $r_i/r_o = 0.5$, 0.75 and 1 (parallel plates), where r_i and r_o are the inner and the outer radii of the duct, respectively. Thermal boundary conditions on solid walls are of the Dirichlet type ($t = t_w$) for all the geometries considered except for the annular ducts where a uniform temperature is imposed on the inner wall, while the outer wall is assumed adiabatic. Thus, the annular duct with $r_i/r_o = 1$ is a parallel plate duct with one adiabatic wall. Computational domains have been defined taking existing symmetries into account. Therefore, for the circular and concentric annular cross-sections the domains are one-dimensional and axisymmetric and have lengths r_o and $r_o - r_i$, respectively. Instead, for the parallel plate channel the domain is a rectangle of unit base and height $a/2$, while for the trapezoidal channel reference is made to the two-dimensional domain of base $b/2$ and height a corresponding to one half of the cross-section. Finally, for the rectangular and hexagonal channels the domains are represented by the regions of base $b/2$ and height $a/2$ corresponding to a quarter of the whole cross-sections.

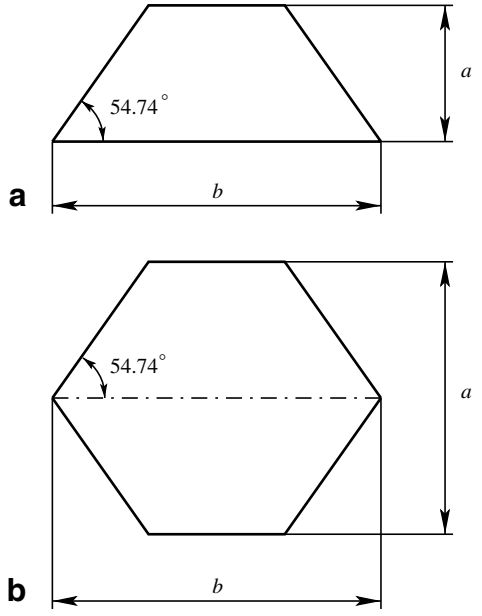

Fig. 2. Schematic representation of two cross-sections used in silicon microchannels: (a) trapezoidal with $\gamma = 0.414$ and (b) hexagonal with $\gamma = 0.828$.

One-dimensional domains have been discretized by means of three-node parabolic elements, while two-dimensional ones have been subdivided into nine-node Lagrangian parabolic elements. A total of 40 elements and 81 nodal points have been used in the discretization of the 1-D domain corresponding to the circular cross-section, and a total of 80 elements and 161 nodal points in that of the 1-D domain corresponding to the concentric annular cross-sections. A total of 50 elements and 303 nodal points have been used in the discretization of the 2-D domain (one row of elements) corresponding to the cross-section of the parallel plate channel, while discretizations of rectangular cross-sections with $\gamma = 0.5$ and 1 have led to meshes with a total of 216 and 225 elements and 925 and 961 nodal points, respectively. Finally, the discretization of the trapezoidal cross-section required 360 elements and 1517 nodal points and that of the hexagonal cross-section 216 elements and 925 nodal points.

In all the meshes, element sizes gradually increase with increasing distance from the walls. The minimum and maximum values of the dimensionless distances between adjacent nodes $\Delta y/D_h$ and $\Delta z/D_h$, or $\Delta r/D_h$, measured in the transverse or in the radial directions, respectively, are reported in Table 1 for all the cross-sectional geometries considered. The adopted meshes are fine enough near the walls to allow an accurate representation of the steep velocity and temperature gradients taking place there as the flow

Table 1
Minimum and maximum values of the dimensionless distances between adjacent nodes $\Delta y/D_h$ and $\Delta z/D_h$, or $\Delta r/D_h$, in the finite element meshes employed for the numerical simulations

Cross-section	$\Delta y_{min}/D_h$ or $\Delta r_{min}/D_h$	$\Delta z_{min}/D_h$	$\Delta y_{max}/D_h$ or $\Delta r_{max}/D_h$	$\Delta z_{max}/D_h$
Circular	0.0003	–	0.0122	–
Parallel plates	0.0001	–	0.0041	–
Square	0.0062	0.0062	0.0247	0.0247
Rectangular	0.0066	0.0069	0.0247	0.0310
Trapezoidal	0.0029	0.0039	0.0580	0.0428
Hexagonal	0.0019	0.0023	0.0449	0.0252
Annular (all r_i/r_o)	0.0002	–	0.0061	–

develops. Of course, preliminary tests had been carried out to verify that all these discretizations are fine enough to give mesh-independent results. In all the computations, the axial step has gradually been increased from the starting value $\Delta x/D_h = 0.0001$ to the maximum value $\Delta x/D_h = 0.5$. As the initial value of the axial step is very small, the strong variations of the axial pressure gradient arising in the first part of the microchannel can be adequately captured.

The procedure outlined in the previous section had already been validated, on the assumption of constant property fluid, by comparing heat transfer and pressure drop results with existing literature data for simultaneously developing laminar flows in straight ducts [12]. In order to assess the accuracy of the present computations, asymptotic values of the Nusselt number $(Nu_\infty)_c$ and fully developed values of the Poiseuille number $(fRe)_c$ for flows of constant property fluids are compared in Table 2 with available literature data. Computed asymptotic values of the Nusselt number for trapezoidal and hexagonal ducts, for which no comparison data are available, are also included in Table 2 for the sake of completeness. Comparison data of $(Nu_\infty)_c$ and $(fRe)_c$ have been found in [1], with the exception of the values of $(fRe)_c$ for trapezoidal and hexagonal ducts which have been taken from [16]. As can be seen, all computed values are in very good agreement with the corresponding literature values, thus confirming the accuracy of present computations.

The effects of temperature dependent viscosity on heat transfer and pressure drop are illustrated here with reference to axial distributions of the local Nusselt number Nu and of the product f_aPe for ducts of different cross-sections. To facilitate the analysis of results, axial distributions of the local Nusselt number Nu_c and of the product $(f_aPe)_c$ for developing constant property flows in three-dimensional ducts (i.e., parallel plate, square, rectangular, trapezoidal and hexagonal ducts) and axisymmetric ducts (i.e., circular and concentric annular ducts) are reported in Figs. 3 and 4, respectively, while axial distributions of the ratios Nu/Nu_c and $f_aPe/(f_aPe)_c$ are presented in Figs. 5–13 for different cross-sectional geometries. Available literature data for $(f_aPe)_c$ from Ref. [1] are also reported for comparison in Figs. 3(b) and 4(b). In all these figures, reference is made to the dimensionless axial coordinate $X^* = x/D_hPe$. This choice, which is standard when axial distributions of Nu are displayed, is made here also for axial distributions of f_aPe, according to [22], because of the temperature dependence of viscosity. It should also be noted that a given value of X^* corresponds to the same physical distance from the inlet for all values of the ratio Pr_e/Pr_w. In order to allow Nu and f_aPe to reach their asymptotic values, the ranges between 0.0001 and 1 and between 0.0001 and 10 of the dimensionless axial coordinate X^* are considered in all figures reporting the axial distributions of Nu and of f_aPe, respectively.

As can be seen by inspection of the axial distributions of Nu_c reported in Figs. 3(a) and 4(a), with constant property liquids almost fully developed conditions are reached at a value of X^* around 0.02 for parallel plates and in the range

Table 2
Comparisons of calculated and literature values of $(Nu_\infty)_c$ and $(fRe)_c$ for constant property flows in ducts of different cross-sections

Cross-section		Circular	Parallel plates	Square	Rectangular	Trapezoidal	Hexagonal	Annular		
γ or r_i/r_o			0	1	0.5	0.414	0.828	0.5	0.75	1
$(Nu_\infty)_c$	Calc.	3.65680	7.54075	2.9775	3.3922	2.7701	3.3247	5.7380	5.1557	4.8616
	Ref.	3.65679	7.54070	2.976	3.391			5.7382		4.8608
$(fRe)_c$	Calc.	16.0000	24.0000	14.2270	15.5480	14.0555	15.0267	23.8125	23.9670	24.0000
	Ref.	16	24	14.2271	15.5481	14.053	15.021	23.813	23.967	24

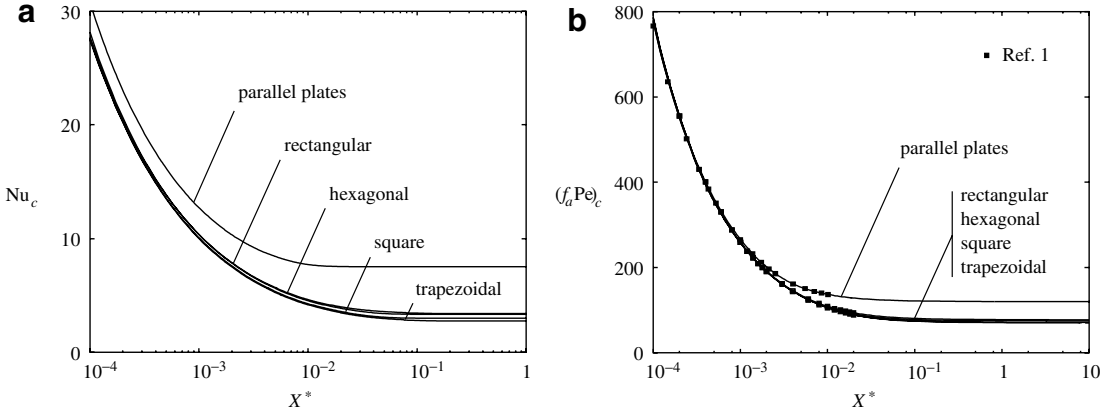

Fig. 3. Flows of constant property fluids with $Pr = 5$ in three-dimensional ducts of different cross-sections (parallel plate, rectangular with $\gamma = 0.5$ and $\gamma = 1$ (square), trapezoidal with $\gamma = 0.414$ and hexagonal with $\gamma = 0.828$): axial distributions (a) of the Nusselt number Nu_c and (b) of the product $(f_aPe)_c$.

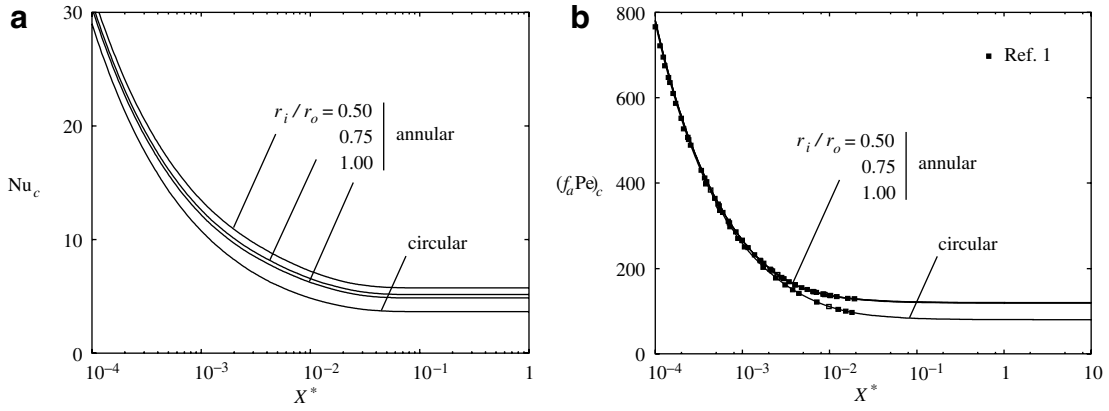

Fig. 4. Flows of constant property fluids with $Pr = 5$ in axisymmetric ducts of different cross-sections (circular and concentric annular with $r_i/r_o = 0.5$, $r_i/r_o = 0.75$ and $r_i/r_o = 1$ (parallel plates)): axial distributions (a) of the Nusselt number Nu_c and (b) of the product $(f_aPe)_c$.

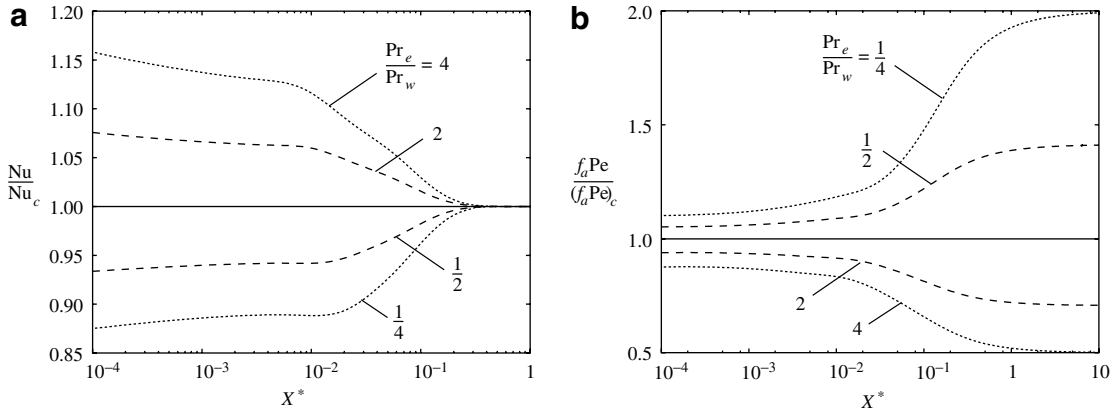

Fig. 5. Flows of temperature dependent viscosity fluids with $Pr_m = 5$ in ducts of circular cross-section: axial distributions (a) of the ratio Nu/Nu_c and (b) of the ratio $f_aPe/(f_aPe)_c$.

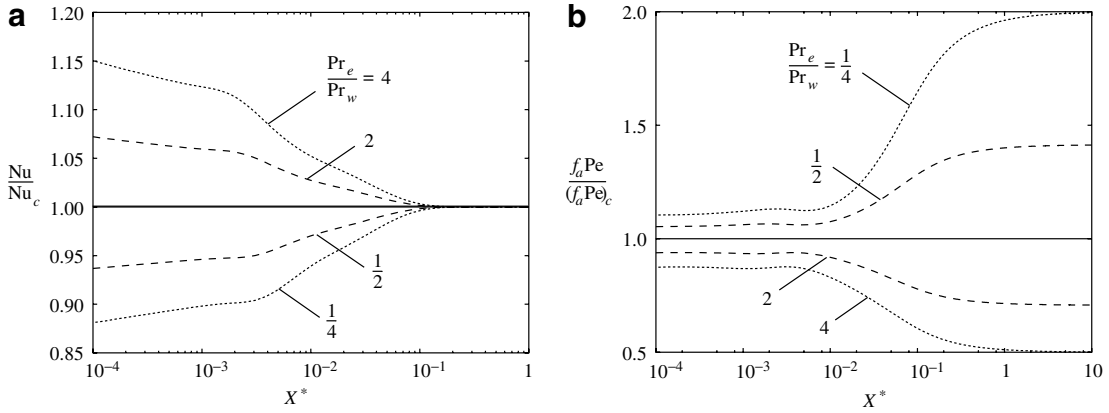

Fig. 6. Flows of temperature dependent viscosity fluids with $Pr_m = 5$ in parallel plate ducts: axial distributions (a) of the ratio Nu/Nu_c and (b) of the ratio $f_aPe/(f_aPe)_c$.

between 0.05 and 0.1 for the other geometries. The same conclusions can be reached after inspecting the axial distributions of $(f_aPe)_c$ reported in Figs. 3(b) and 4(b). Axial distributions of Nu_c for circular, rectangular, trapezoidal and hexagonal cross-sectional geometries are very similar, leading to fully developed values of the Nusselt number $(Nu_\infty)_c$ ranging between 2.77 (trapezoidal) and 3.66 (circular), while the parallel plate duct exhibits a rather different behaviour ($(Nu_\infty)_c = 7.54$). Similar axial distributions of Nu_c are also found for the concentric annular ducts

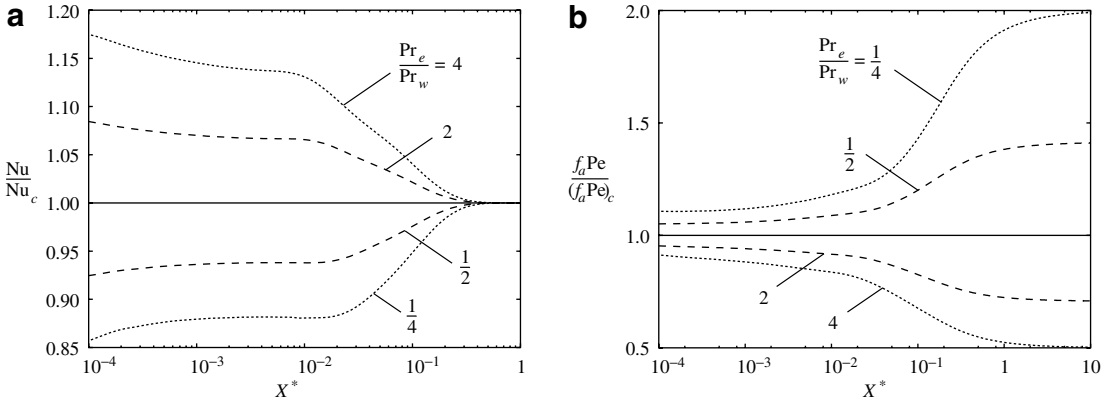

Fig. 7. Flows of temperature dependent viscosity fluids with $Pr_m = 5$ in rectangular ducts with $\gamma = 1$ (square ducts): axial distributions (a) of the ratio Nu/Nu_c and (b) of the ratio $f_aPe/(f_aPe)_c$.

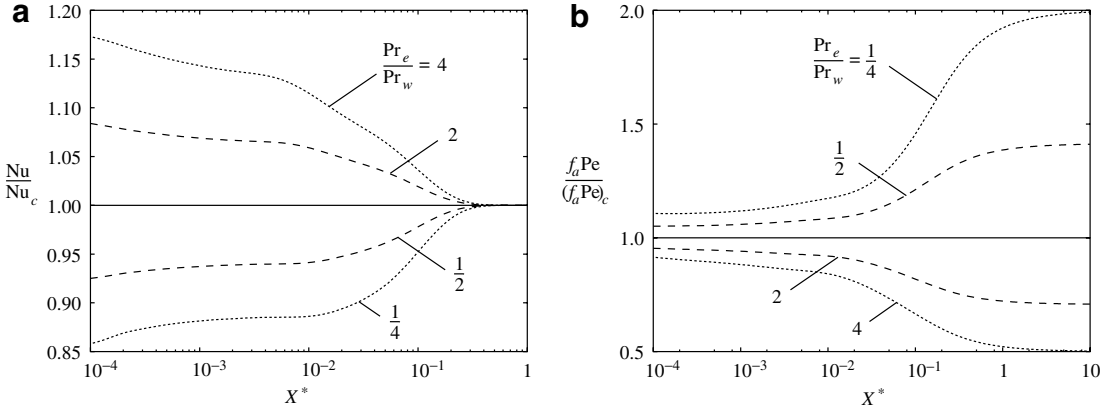

Fig. 8. Flows of temperature dependent viscosity fluids with $Pr_m = 5$ in rectangular ducts with $\gamma = 0.5$: axial distributions (a) of the ratio Nu/Nu_c and (b) of the ratio $f_aPe/(f_aPe)_c$.

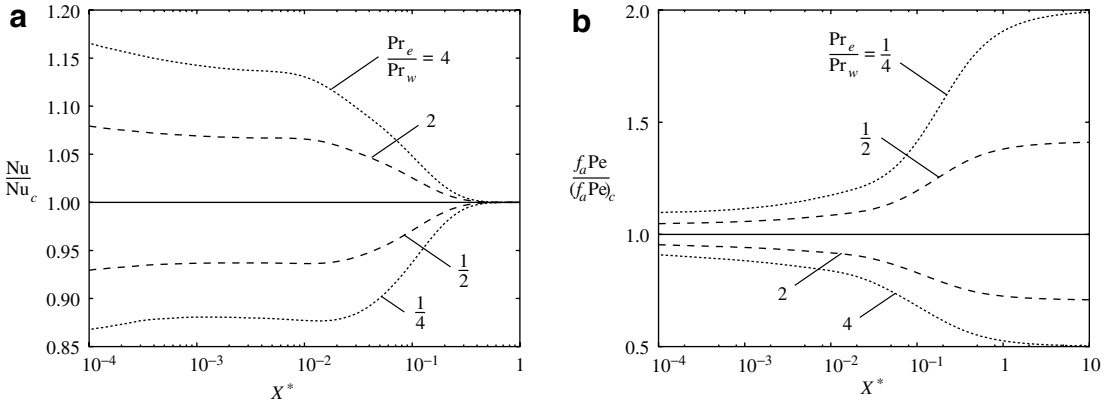

Fig. 9. Flows of temperature dependent viscosity fluids with $Pr_m = 5$ in trapezoidal ducts with $\gamma = 0.414$: axial distributions (a) of the ratio Nu/Nu_c and (b) of the ratio $f_aPe/(f_aPe)_c$.

considered here, whose values of $(Nu_\infty)_c$ range between 4.86 and 5.73. As can be seen in Fig. 3(b) and Fig. 4(b), axial distributions of $(f_aPe)_c$ are nearly the same for ducts of circular, rectangular, trapezoidal and hexagonal cross-sections, with fully developed $(fPe)_c$ ranging between 70.26 and 80.00, and for parallel plates and the concentric annular ducts considered here, with fully developed $(fPe)_c$ ranging between 119.07 and 120.00.

The effects of temperature dependent viscosity on the local Nusselt number are illustrated in Figs. 5(a)–13(a),

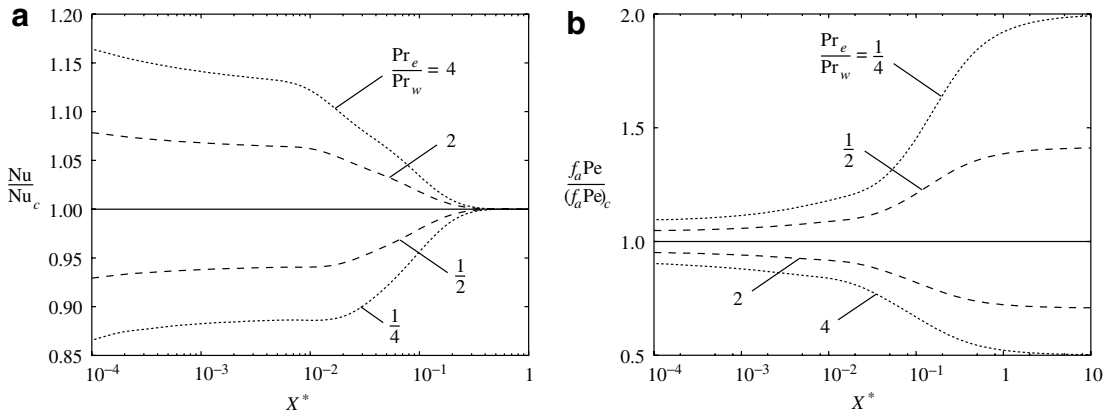

Fig. 10. Flows of temperature dependent viscosity fluids with $Pr_m = 5$ in hexagonal ducts with $\gamma = 0.828$: axial distributions (a) of the ratio Nu/Nu_c and (b) of the ratio $f_aPe/(f_aPe)_c$.

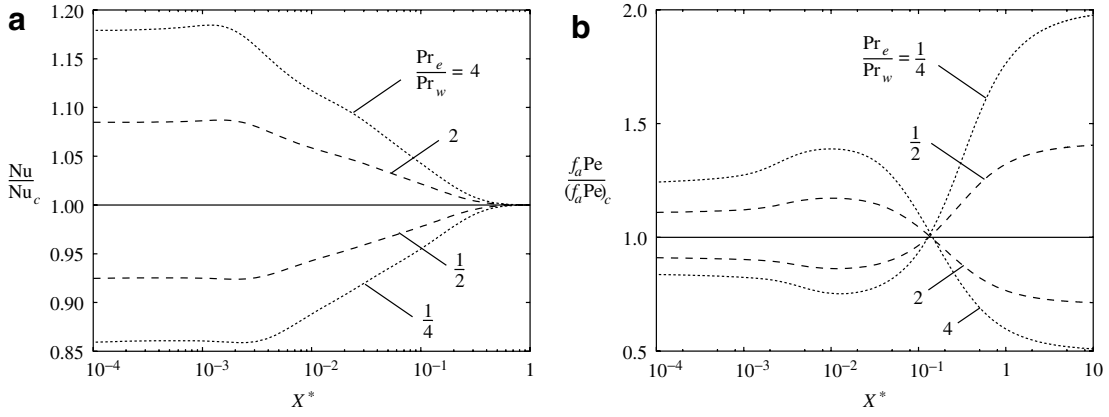

Fig. 11. Flows of temperature dependent viscosity fluids with $Pr_m = 5$ in concentric annular ducts with $r_i/r_o = 0.5$: axial distributions (a) of the ratio Nu/Nu_c and (b) of the ratio $f_aPe/(f_aPe)_c$.

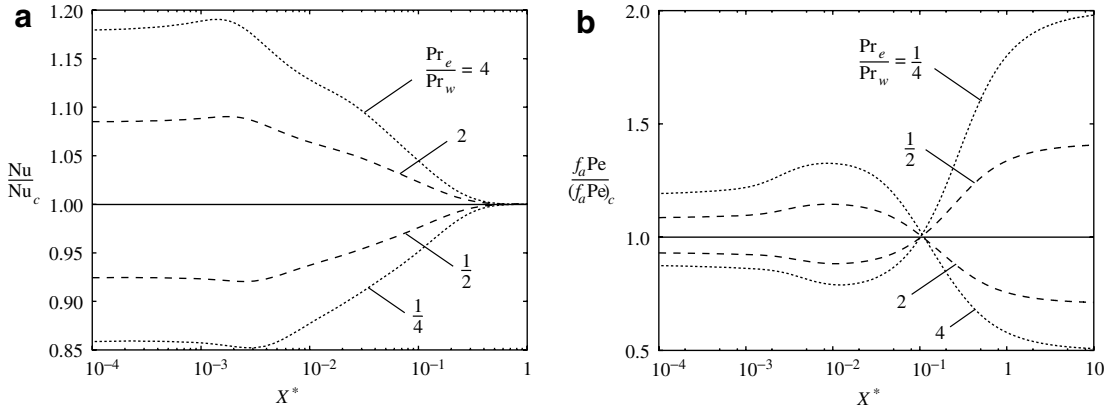

Fig. 12. Flows of temperature dependent viscosity fluids with $Pr_m = 5$ in concentric annular ducts with $r_i/r_o = 0.75$: axial distributions (a) of the ratio Nu/Nu_c and (b) of the ratio $f_aPe/(f_aPe)_c$.

where axial distributions of the ratio Nu/Nu_c for ducts of different cross-sections are presented. As can be seen, the ratio Pr_e/Pr_w significantly affects the Nusselt number as long as the flow develops, while its influence gradually decreases as isothermal flow conditions are approached. These conditions are reached at values of X^* in the ranges between 0.1 and 0.2 for parallel plates and between 0.2 and 0.5 for the other geometries, i.e, at values of X^* significantly higher than those of the thermal entrance lengths in the corresponding flows of constant property fluids. The

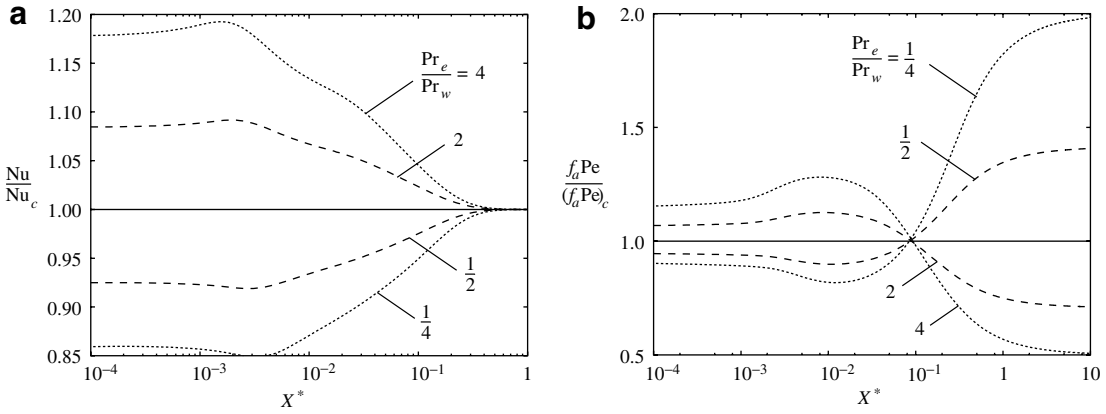

Fig. 13. Flows of temperature dependent viscosity fluids with $Pr_m = 5$ in concentric annular ducts with $r_i/r_o = 1$ (parallel plates): axial distributions (a) of the ratio Nu/Nu_c and (b) of the ratio $f_aPe/(f_aPe)_c$.

comparison of axial distributions of Nu/Nu_c for a given cross-sectional geometry and different values of the ratio Pr_e/Pr_w shows the same qualitative behaviour. The values of Nu/Nu_c are always larger that 1 for fluid heating ($Pr_e/Pr_w > 1$) and smaller than 1 for fluid cooling ($Pr_e/Pr_w < 1$). All curves reach unity for sufficiently large values of X^*. However, there is a noticeable change in the slope of the curves around $X^* = 0.003$ for parallel plates and concentric annular ducts and around $X^* = 0.02$ for the other geometries. We verified that this change in the slope of the Nu/Nu_c profiles always occurs at the axial position where the value of temperature at the duct axis t_0 starts departing from t_e, i.e., where the thermal boundary layers developing on opposite walls of the ducts meet together.

The effects of temperature dependent viscosity on the apparent friction factor are illustrated in Figs. 5(b)–13(b), where axial distributions of the ratio $f_aPe/(f_aPe)_c$ for ducts of different cross-sections are presented. As can be seen, asymptotic values $[f_aPe/(f_aPe)_c]_\infty$ of the ratio $f_aPe/(f_aPe)_c$ only depend on Pr_e/Pr_w, no matter which cross-sectional geometry is considered. In fact, we can write

$$\left[\frac{f_aPe}{(f_aPe)_c}\right]_\infty = \frac{fPe}{(fPe)_c} = \frac{fRe_wPr_w}{(fRe)_cPr_m} = \frac{Pr_w}{Pr_m} \tag{17}$$

since it is $fRe_w = (fRe)_c = C$, where C is a constant whose value depends on the particular cross-sectional geometry considered [1]. Therefore, the asymptotic values $[f_aPe/(f_aPe)_c]_\infty = 2, \sqrt{2}, 1/\sqrt{2}$ and 1/2 are obtained for $Pr_e/Pr_w = 1/4$, 1/2, 2 and 4, respectively, as shown in Figs. 5(b)–13(b). Instead, in the region close to the entrance, similar axial distributions of $f_aPe/(f_aPe)_c$ are obtained for different cross-sectional geometries (see Figs. 5(b)–10(b)), with the exception of concentric annular ducts with the outer wall adiabatic, which exhibit a very different behaviour (see Figs. 11(b)–13(b)). As expected, we always have $f_aPe/(f_aPe)_c > 1$ for fluid cooling ($Pr_e/Pr_w < 1$, that is, $Pr_w/Pr_m > 1$) and $f_aPe/(f_aPe)_c < 1$ for fluid heating ($Pr_e/Pr_w > 1$, that is, $Pr_w/Pr_m < 1$). In fact, in the first case the pressure drop is higher than that corresponding to the flow of a constant property fluid, due to the higher values of viscosity in the near wall region ($\mu_w > \mu_m$), while the opposite occurs in the second case ($\mu_w < \mu_m$). Since the effect of the ratio Pr_e/Pr_w increases for increasing X^*, the profiles of $f_aPe/(f_aPe)_c$ tend to diverge from unity, at first slightly, up to a value of X^* around 0.01 for parallel plates and around 0.05 for the other geometries, and then more markedly, up to $X^* \cong 1$. As already pointed out, a different behaviour is observed in the regions close to the entrance of concentric annular ducts with the outer wall adiabatic, where we have $f_aPe/(f_aPe)_c < 1$ for fluid cooling and $f_aPe/(f_aPe)_c > 1$ for fluid heating. This behaviour can be explained if we consider that the pressure drop depends on shear stresses acting both at the inner and outer walls, which in turn depend on local temperatures through the corresponding values of viscosity. Since in the first part of the duct the fluid temperature is close to t_w near the inner wall and is equal to t_e near the outer wall, which is adiabatic, the flow is almost isothermal near the outer wall, while a (thin) thermal boundary layer is developing along the inner wall. The influence of the adiabatic wall on the pressure drop prevails over that of the wall maintained at t_w, thus producing the above mentioned behaviour. After the flow develops enough (beyond $X^* = 0.01$) to cause the fluid temperature at the outer wall to become close to t_w, the influence of the inner wall starts prevailing, thus leading to the same behaviour observed for the other cross-sectional geometries when isothermal conditions are approached.

The differences between the local values of Nu/Nu_c and $f_aPe/(f_aPe)_c$ found for different values of the ratio Pr_e/Pr_w can be explained taking into account velocity and temperature distributions over the cross-sections. Radial profiles of the dimensionless axial velocity $U = u/u_e$ and of the dimensionless temperature $T = (t - t_w)/(t_e - t_w)$ at selected axial locations for the considered values of Pr_e/Pr_w are reported in Figs. 14–16 for circular ducts, concentric annular ducts with $r_o/r_i = 0.5$ and parallel plate channels. Variables $R = r/r_o$ and $Z = z/D_h$ represent the dimensionless radial and transverse coordinates, respectively. In order to consider comparable situations, dimensionless velocity

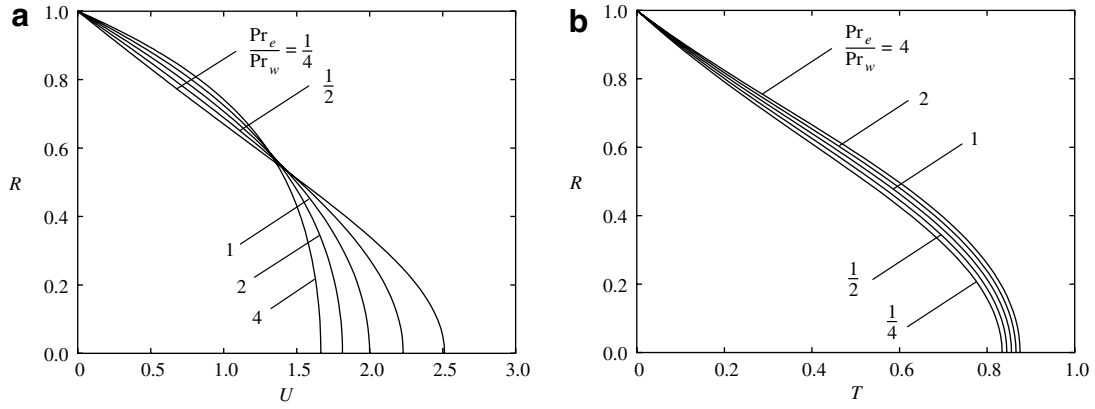

Fig. 14. Flows of temperature dependent viscosity fluids with $Pr_m = 5$ in ducts of circular cross-section: radial profiles at the axial positions where $T_b = 0.5$ of (a) dimensionless velocity U and (b) dimensionless temperature T for different values of the ratio Pr_e/Pr_w.

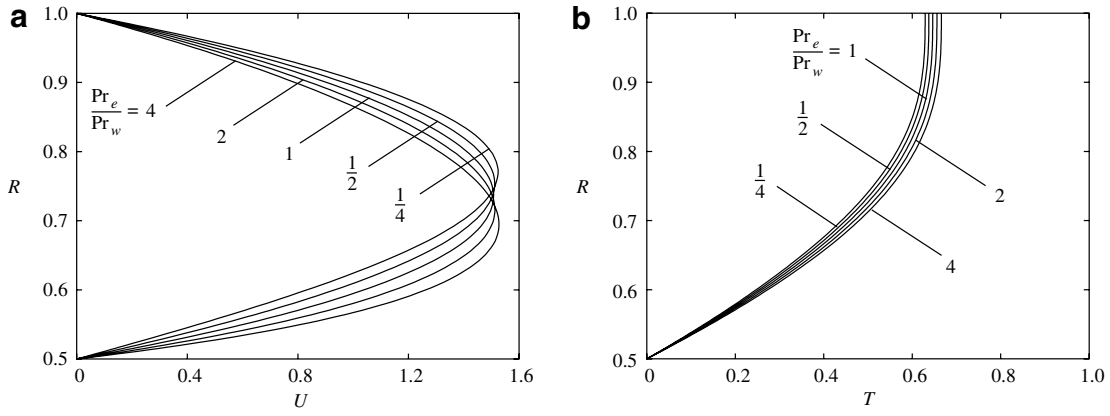

Fig. 15. Flows of temperature dependent viscosity fluids with $Pr_m = 5$ in concentric annular ducts with $r_i/r_o = 0.5$: radial profiles at the axial positions where $T_b = 0.5$ of (a) dimensionless axial velocity U and (b) dimensionless temperature T for different values of the ratio Pr_e/Pr_w.

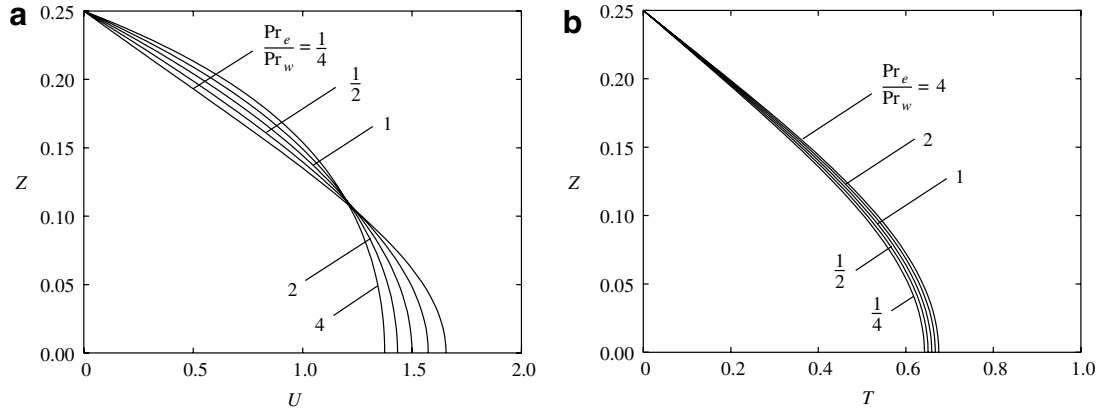

Fig. 16. Flows of temperature dependent viscosity fluids with $Pr_m = 5$ in parallel plate ducts: profiles in the transverse direction at the axial positions where $T_b = 0.5$ of (a) dimensionless axial velocity U and (b) dimensionless temperature T for different values of the ratio Pr_e/Pr_w.

and temperature profiles reported in Figs. 14–16 refer to cross-sections where the bulk temperature t_b coincides with the reference temperature of the fluid t_m, so that $T_b = (t_b - t_w)/(t_e - t_w) = 0.5$. For $Pr_e/Pr_w = 4$, 2, 1, 1/2 and 1/4, the corresponding values of the dimensionless axial coordinate are $X^* = 0.02900$, 0.03113, 0.03354, 0.03615 and 0.03894 for circular ducts, $X^* = 0.07229$, 0.07615, 0.08015, 0.08416 and 0.08819 for concentric annular ducts with $r_o/r_i = 0.5$ and $X^* = 0.01808$, 0.01884, 0.01967, 0.02052 and 0.02129 for parallel plate channels, respectively.

As can be seen, viscosity variations with temperature significantly affect the values of velocity and temperature gradients at the duct walls, leading to rather different Nusselt numbers and apparent friction factors, as discussed above. Similar conclusions can be reached by looking at Fig. 17, where transverse distributions of the dimensionless velocity U, at the axial position where $T_b = 0.5$, are shown for three-dimensional flows in ducts of trapezoidal cross-section. The corresponding values of the dimensionless axial coordinate are $X^* = 0.03490$, 0.04108 and 0.04877 for $Pr_e/Pr_w = 4$,1 and 1/4, respectively.

To show the influence of the temperature dependence of viscosity on the hydrodynamic entrance length, the axial distributions of dimensionless velocity U_0 and temperature T_0 at the center of the cross-section of circular ducts and parallel plate channels are presented in Fig. 18 for all the values of Pr_e/Pr_w considered. It must be pointed out that these cross-sectional geometries represent the limiting cases

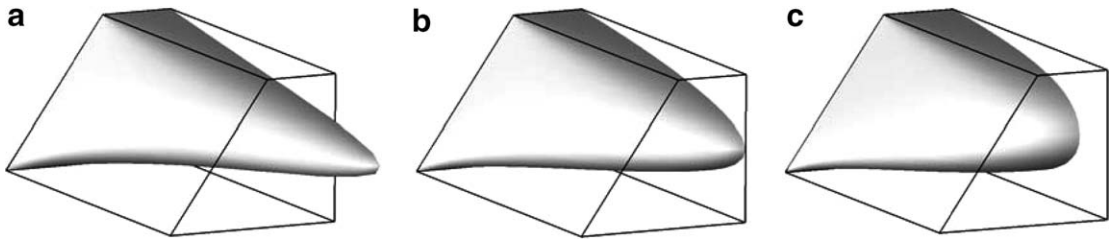

Fig. 17. Flows of temperature dependent viscosity fluids with $Pr_m = 5$ in trapezoidal ducts: transverse distributions of the dimensionless axial velocity U at the axial positions where $T_b = 0.5$ for (a) $Pr_e/Pr_w = 1/4$, (b) $Pr_e/Pr_w = 1$ and (c) $Pr_e/Pr_w = 4$.

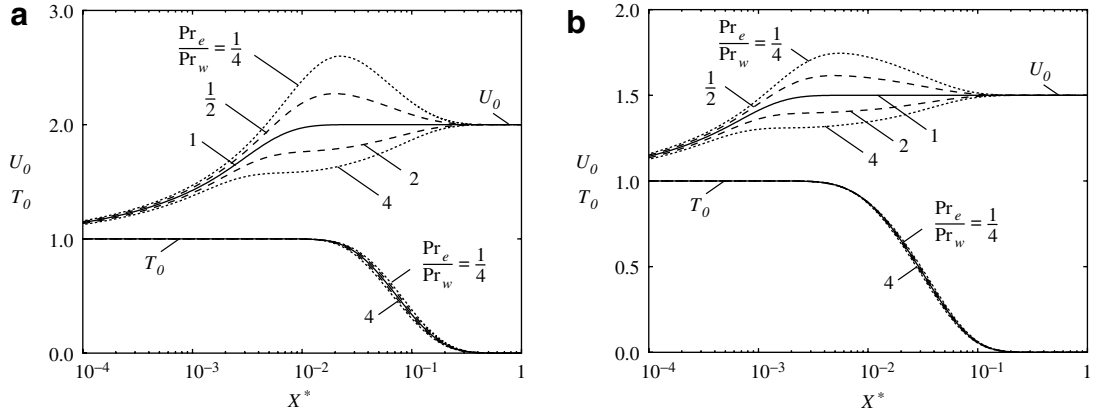

Fig. 18. Flows of temperature dependent viscosity fluids with $Pr_m = 5$: axial distributions of the dimensionless velocity U_0 and of the temperature T_0 at the center of the cross-section for (a) circular ducts and (b) parallel plate channels.

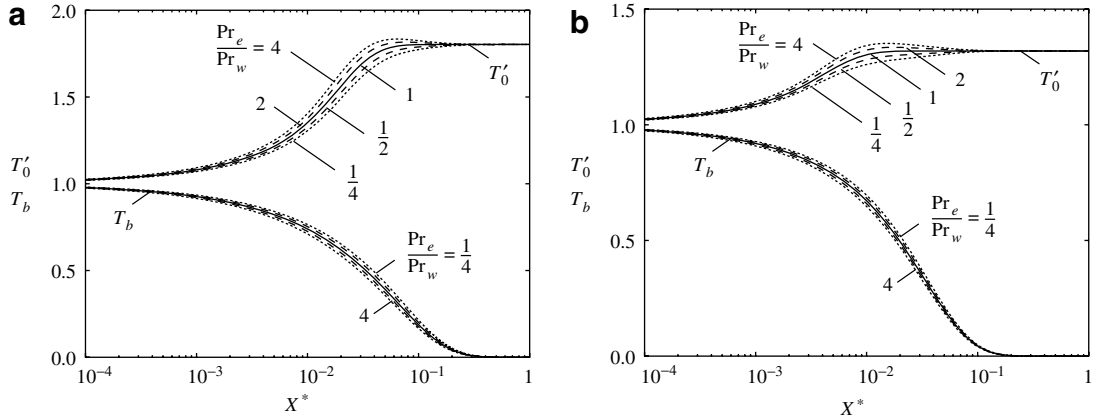

Fig. 19. Flows of temperature dependent viscosity fluids with $Pr_m = 5$: axial distributions of the dimensionless centerline temperature $T_0' = (t_0 - t_w)/(t_b - t_w)$ and of the dimensionless bulk temperature T_b for (a) circular ducts and (b) parallel plate channels.

corresponding to the maximum and minimum values of the ratio P/A of the wetted perimeter over the area of the cross-section. Therefore, an intermediate behaviour can be expected for ducts with different cross-sectional geometries. It is apparent that, in the case of temperature dependent viscosity, fully developed values of the dimensionless axial velocity component U_0 are reached only where the flow becomes nearly isothermal, that is, at the distance from the inlet where the centerline temperature approaches the wall temperature. This distance appears to be nearly independent of the value of Pr_e/Pr_w and is about one order of magnitude larger than the hydrodynamic entrance length in the corresponding constant property flow [1,2,23]. We can also notice that the value of U_0 is lower than its asymptotic value everywhere in the case of fluid heating, while it exhibits an overshoot in the case of fluid cooling. Besides, the more the ratio Pr_e/Pr_w differs from 1, the larger the differences are between local values of U_0 for flows of fluids with temperature dependent viscosity and the corresponding values for flows of constant property fluids.

Finally, the axial distributions of the dimensionless centerline temperature $T'_0 = (t_0 - t_w)/(t_b - t_w)$ and of the dimensionless bulk temperature T_b are reported in Fig. 19 with reference to the same cross-sectional geometries and values of Pr_e/Pr_w considered in Fig. 18. It is apparent that, in the case of temperature dependent viscosity, also thermally fully developed conditions, characterized by constant values of T'_0, i.e., by $dT'_0/dX^* = 0$, are reached where the fluid is nearly at the wall temperature, at distances from the inlet which are about one order of magnitude larger than thermal entrance lengths for the corresponding constant property flows.

4. Conclusions

A parametric investigation has been carried out on the effects of temperature dependent viscosity in simultaneously developing laminar flow of a liquid in straight ducts of arbitrary but constant cross-sections. Viscosity has been assumed to vary with temperature according to an exponential relation, while the other fluid properties have been held constant. Different cross-sectional geometries have been considered, corresponding both to axisymmetric (circular and concentric annular) and to three-dimensional (rectangular, trapezoidal and hexagonal) duct geometries. Reference has been made to uniform wall temperature boundary conditions. Numerical results confirm that, in the laminar forced convection in the entrance region of straight ducts, the effects of temperature dependent viscosity cannot be neglected in a wide range of operative conditions.

Acknowledgement

This work was funded by MIUR (PRIN/COFIN 2003 and 2005 projects).

References

[1] R.K. Shah, A.L. London, Laminar Flow Forced Convection in Ducts, Academic Press, New York, 1978.
[2] R.K. Shah, M.S. Bhatti, Laminar convective heat transfer in ducts, in: S. Kakaç, R.K. Shah, W. Aung (Eds.), Handbook of Single-Phase Convective Heat Transfer, Wiley, New York, 1987, Chapter 3.
[3] S. Kakaç, The effect of temperature-dependent fluid properties on convective heat transfer, in: S. Kakaç, R.K. Shah, W. Aung (Eds.), Handbook of Single-Phase Convective Heat Transfer, Wiley, New York, 1987, Chapter 18.
[4] C. Nouar, Numerical solution for laminar mixed convection in a horizontal annular duct: temperature-dependent viscosity effect, Int. J. Numer. Meth. Fluids 29 (1999) 849–864.
[5] J.M. Nóbrega, F.T. Pinho, P.J. Oliveira, O.S. Carneiro, Accounting for temperature dependent properties in viscoelastic duct flows, Int. J. Heat Mass Transfer 47 (2004) 1141–1158.
[6] R.L. Shannon, C.A. Depew, Forced laminar flow convection in a horizontal tube with variable viscosity and free convection effects, J. Heat Transfer 91 (1969) 251–258.
[7] S.D. Joshi, A.E. Bergles, Analytical study of heat transfer to laminar in-tube flow of non-Newtonian fluids, AIChE Symp. Ser. 76 (199) (1980) 270–281.
[8] K.C. Toh, X.Y. Chen, J.C. Chai, Numerical computation of fluid flow and heat transfer in microchannels, Int. J. Heat Mass Transfer 45 (2002) 5133–5141.
[9] B. Xu, K.T. Ooi, C. Mavriplis, M.E. Zaghloul, Evaluation of viscous dissipation in liquid flow in microchannels, J. Micromech. Microeng. 13 (2003) 53–57.
[10] J. Koo, C. Kleinstreuer, Viscous dissipation effects in microtubes and microchannels, Int. J. Heat Mass Transfer 47 (2004) 3159–3169.
[11] J. Koo, C. Kleinstreuer, Analysis of liquid flow in micro-conduits, in: Proc. of the 2nd ICMM, Rochester, NY, 2004, pp. 191–198.
[12] C. Nonino, S. Del Giudice, G. Comini, Laminar forced convection in three-dimensional duct flows, Numer. Heat Transfer 13 (1988) 451–466.
[13] S.V. Patankar, D.B. Spalding, A calculation procedure for heat, mass and momentum transfer in three-dimensional parabolic flows, Int. J. Heat Mass Transfer 15 (1972) 1787–1806.
[14] C. Hirsh, Numerical Computation of Internal and External Flows, vol. 1, Wiley, New York, 1988, p. 70.
[15] G.L. Morini, Viscous dissipation as scaling effect for liquid flows in microchannels, in: Proc. of the 3rd ICMM, Toronto, 2005.
[16] G.L. Morini, Viscous heating in liquid flows in microchannels, Int. J. Heat Mass Transfer 48 (2005) 3637–3647.
[17] C.R. Lin, C.K. Chen, Effect of temperature dependent viscosity on the flow and heat transfer over an accelerating surface, J. Phys. D: Appl. Phys. 27 (1994) 29–36.
[18] A. Costa, G. Macedonio, Nonlinear phenomena in fluids with temperature-dependent viscosity: an hysteresis model for magma flow in conduits, Geophys. Res. Lett. 29 (10) (2002). Art. No. 1402.
[19] A. Costa, G. Macedonio, Viscous heating for fluids with temperature dependent viscosity: implications for magma flows, Nonlinear Processes Geophys. 10 (2003) 545–555.
[20] V. Javeri, Heat transfer in laminar entrance region of a flat channel for the temperature boundary condition of the third kind, Wärme-Stoffübertragung 10 (1977) 137–144.
[21] C. Nonino, A simple pressure stabilization for a SIMPLE-like equal-order FEM algorithm, Numer. Heat Transfer, Part B 44 (2003) 61–81.
[22] M.W. Collins, Viscous dissipation effects on developing laminar flow in adiabatic and heated tubes, Proc. Instn. Mech. Engrs. 189 (15/75) (1975) 129–137.
[23] F. Durst, S. Ray, B. Ünsal, O.A. Bayoumi, The development lengths of laminar pipe and channel flows, J. Fluids Eng. 127 (2005) 1154–1160.